Chinese Journal of Polymer Science Vol. 32, No. 4, (2014), 497–508

Chinese Journal of Polymer Science

Dielectric Investigations on How Mg Salt Is Dispersed in and Released from Polylactic Acid*

Yu-jie Cao[a], Dan Zhu[a**], To Ngai[b], Ling Qin[c], Chi Wu[b] and Jian Shen[a]

[a] *Jiangsu Key Laboratory of Bio-functional Materials, College of Chemistry and Materials Science, Nanjing Normal University, Nanjing 210046, China*

[b] *Department of Chemistry, The Chinese University of Hong Kong, Shatin N.T., Hong Kong*

[c] *The Musculoskeletal Research Laboratory, Department of Orthopaedics and Traumatology, The Chinese University of Hong Kong, Shatin N.T., Hong Kong*

Abstract Composite biomaterials made of biodegradable polylactic acid (PLA) and bioactive magnesium (Mg) salt are developed for orthopaedic implants or metal implant coatings. The releasing of Mg salt into the biological environment benefits the bone growth, while with the releasing of Mg salt and degradation of PLA there forms a porous scaffold for tissue engineering. The size and morphology of the salt and voids are adjustable with such preparation conditions as salt content, pH of casting solution, and the solidification rate, so that we can control the salt releasing and degradation rate of PLA. Dielectric spectroscopy is used to investigate the dispersive structures of Mg salt and voids in the polymer matrix and to monitor the *in situ* releasing of Mg salts in the simulated body fluid (SBF). The current study provides us with an orthopedic biomaterial with controllable multi-phase structures, and a tool to investigate the *in vivo* behaviors of biomaterials.

Keywords: Dielectric spectroscopy; Inorganic-polymer composite; Orthopaedic biomaterials; Biodegradation; Bioactivity.

INTRODUCTION

The distinguished feature of biodegradability has endowed polylactic acid (PLA) with promising applications in orthopaedic biomaterials, such as fixation matrix, drug delivery carriers, tissue scaffold and protective implant coatings[1, 2]. It also possesses the advantages of polymeric material such as easy and adjustable fabrications for desired thickness and complex shapes. Nowadays intelligence or multi-functionality is more desired for biomaterials to adapt the complex biological environment[3, 4], so the composite of PLA and the inorganic or organic materials is extensively studied, such as the composite of PLA and hydroxyapatite (HAP, $Ca_{10}(PO_4)_6(OH)_2$) or tricalcium phosphate (TCP, $Ca_3(PO_4)_2$) used as orthopaedic implants, cardiovascular implants coated with PLA and incorporated with thrombin inhibitor, and drug eluting stents or stent coating[5, 6]. Magnesium (Mg) is an important element of bone matrix and an important cofactor for many enzymes involving in bone resorption and formation. Mg and its alloys have been considered excellent orthopaedic implant biomaterials because of their proper mechanical properties which may avoid stress shielding, degradation and re-operation, and magnesium ion (Mg^{2+}) provided in its degradation can promote bone growth[7, 8], because it adjusts enzymatic activities and adenosine triphosphate storage in the cells, makes the osteogenitor cells more attachable and differentiated, and at the same time, enhances the mineral depositing[9, 10]. A composite coating of

* This work was financially supported by the National Natural Scientific Foundation of China (Nos. 50773077, 20934005 and 51273091) and the Hong Kong Special Administration Region Earmarked Projects (CUHK4042/09P, 2160396).

** Corresponding author: Dan Zhu (朱丹), E-mail: zhudan@njnu.edu.cn

Received August 12, 2013; Revised December 13, 2013; Accepted December 24, 2013
doi: 10.1007/s10118-014-1421-1

PLA and Mg salt will effectively increase the corrosion resistance of Mg/Mg alloys in a simulated body fluid and make them more suitable for orthopaedic applications, while at the same time the coating can provide the short-term release of Mg^{2+} that promotes the bone growth.

Therefore, we have designed and developed a novel composite biomaterial made of PLA and Mg salt, which can provide mechanical supporting in the short-term after the surgery, and it also can provide the porous structure suitable for bone tissue engineering in a long time after the salt dissolution. Specifically, the controlled release of Mg ions with precise level and/or location will improve the efficiency and selectivity of the orthopaedic therapies. However a precise control of the resultant morphology of a polymer and an inorganic substance remains a challenge in both materials science and engineering, namely, even though polymer composites have been extensively developed over the last few decades and entered our every day's modern life, we do not fully understand how to precisely manipulate their multi-level structures, including heterogeneities in their composition, phase and interface morphology, which are originated from synthetic or engineering process or both[11, 12].

In most applications of biomaterials, the surface properties are of significant importance and a bioactive coating layer is necessary. Considering that some orthopaedic implants have complicated shapes, we have decided to use the solution casting method. We have also purposely chosen a mixture of 1,4-dioxane and water as the solvent on considering the potential cellular and tissue toxicities. We have tried to optimize the morphology of the PLA/$MgAc_2$ composites with the electrical and other characterizations by varying the initial PLA and salt concentrations and their weight ratio, the solution pH, the solvent composition (ratio of 1,4-dioxane and water), the solution and drying temperatures, the standing time of the solution mixture before it is cast, and the solvent evaporation rate. We have considered that both thermodynamics and kinetics affect the resultant morphology. The experimental results have shown how the dispersion (amount and morphology) of Mg salt and voids inside PLA is affected by the salt content in the composite, the film casting (solidification) rate, and the pH of the salt solution, namely with increasing salt content and pH of the salt solution, the porosity of the composite increases, with decreasing the volatile rate of the solvent, the porosity increases while the salt phase regions become connected. The evaluated dielectric properties are closely correlated with the heterogeneous multi-phase structures, which can be adjusted by the preparation conditions mentioned above.

In the current study, we have mainly used dielectric relaxation spectroscopy, an old but powerful tool, to characterize the heterogeneous structures of the composites[13, 14]. In an applied field, a complicated heterogeneous system, such as a polymer composite with phases of different components or condensed states, shows the frequency- and temperature- dependent permittivity sensitive to such structural information as the content and morphology of the multi-phases[13, 15–19]. The dielectric and electric properties of prepared PLA/$MgAc_2$ composites strongly depend on how Mg salt and voids are dispersed inside PLA, *i.e.*, the amount and the domain size of the salt and void phases. We have also used dielectric relaxation spectroscopy to study the releasing of Mg salt in the water, and after the salt is dissolved out, the permittivity and conductivity of both the water and the film will increase, since the voids of film is filled with water. The relaxation time of the interfacial polarization becomes short after salt releasing.

EXPERIMENTAL

Materials

PLA (PLLA, AI-1001, M_w = 100000 g/mol) with a density of 1.25 g/cm^3 was purchased from Shenzhen Esun Industrial Co., Ltd. Other reagents and solvent used were of analytical grade.

Preparation of PLA/$MgAc_2$ Films

The films were prepared by mixing a 1,4-dioxane solution of PLA and an aqueous solution of $MgAc_2$ together, then injecting the solution mixture into a Teflon dish in a stove with defined ambient temperatures. More specifically, PLA and $MgAc_2$ were first dissolved in 1,4-dioxane (0.2 g/mL) and water (0.1–0.3 g/mL), respectively, and they were mixed with a volume ratio of 9:1. Note that 1,4-dioxane and water are 100%

miscible. Each kind of such prepared films with different salt contents was dried in an oven at different temperatures (30, 50 or 70 °C). Knowing densities and concentrations of PLA and Mg salts, we were able to control the film thickness in the range of 30–300 μm. Each of such prepared film was further cut into *ca*. 20 pieces with a diameter of 2.0 cm with a round blade for dielectric and other measurements.

Dielectric Relaxation Measurements

A broadband dielectric spectrometer (Novocontrol Technologies, BDS40, Germany) with a ZGS extension test interface was used to characterize dielectric and electric behaviors of PLA/$MgAc_2$ films before and after they were immerged in the simulated body fluid (SBF, D-Hanks without Ca^{2+} nor Mg^{2+}). In each measurement, the film was cut with a designed protocol blade with the diameter of 2 cm, each surface was coated with silver conductive paint (CW-200B, CAIG Laboratories Co., USA), then tightly sandwiched in two Au-coated copper electrodes, as shown in Fig. 1(a). The *in situ* measurement of the dissolution of Mg salts in water was recorded with a home-made cell, as shown in Fig. 1(b). An ac voltage 1.5 V (rms) with a frequency range 10^{-2}–10^{7} Hz was applied. All the measurements were performed at the room temperature.

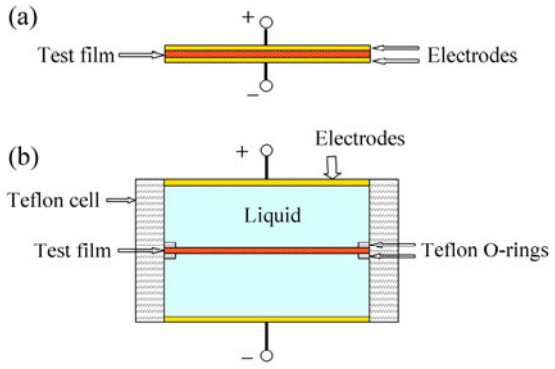

Fig. 1 Schematic of dielectric cells: (a) dry cell and (b) liquid cell

Scanning Electron Microscopy (SEM)

The surface and cross section of PLA/$MgAc_2$ films were imaged by SEM (JSM-5610LV, JEOL, Japan). The cross section was formed from the fracture in liquid nitrogen. A voltage of 15 kV was applied. Each sample was Pt plated before its measurements. Both secondary electron images (SEI) and back-scattered electron images (BSEI) were used. The former was used to image the surface morphology, while the latter, mainly for the compositional distribution.

Elementary Analysis

The elements in the surface composition of the composite films were analyzed by using an energy dispersive X-ray spectroscopy (6692X-1SUS-PL, Thermo Norans). While the dissolved Mg^{2+} concentration in SBF was determined by using an atomic adsorption spectrophotometer (Avanta, GBC), the wavelength used for Mg^{2+} was 285.2 nm.

RESULTS AND DISCUSSION

After searching for a range of solvents, we found that PLA and $MgAc_2$ are respectively soluble in 1,4-dioxane and water, which are 100% miscible. We tried to find the casting temperature above which the phase separation can be avoided. The choice of C_{PLA} = 0.2 g/mL is determined by an adequate viscosity for the film casting. The weight ratio of 1,4-dioxane:water = 9:1 was chosen because more water led to a porous and brittle film; while less water made the salt solution heavier and the blended solution mixture less uniform.

We first prepared the composite films of PLA and $MgAc_2$ with different salt contents in the composite. Figure 2 shows that the resultant film's transparency decreases as the $MgAc_2$ content in the composite increases and the film also becomes brittle, indicating the formation of more large micro-domains (presumably, the

dispersed $MgAc_2$ phase or voids after the removal of water) with a dimension larger than the visible wavelength. We mixed the aqueous $MgAc_2$ solution and PLA solution of 1,4-dioxane at the condition that $C_{PLA} = C_{salt} =$ 0.2 g/mL and their volume ratio was 9:1 at 70 °C. Since the vapor pressure for 1,4-dioxane and water below 100 °C are different, *e.g.*, 16.0 kPa and 12.3 kPa at 50 °C respectively, with the evaporation of the solvents in the oven, the water content in the solvent mixture increases. According to the cloud point recorded for PLA solution in mixture of dioxane and water, the cloud point becomes higher with the increasing of water content in the solvent and also the polymer concentration[20], so that with the film drying in the oven, the water content and PLA concentration increases, liquid-liquid phase separation occurs. With the further solvent evaporation, the polymer is solidified, the solid salt phase appears and the space occupied by the residue solvent will be replaced by the void.

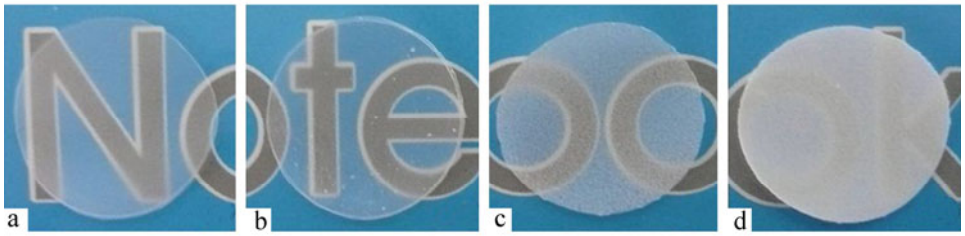

Fig. 2 Appearance of films made of polylactic acid (PLA) and $MgAc_2$ composites with $MgAc_2$: PLA of (a) 0 wt%, (b) 10 wt%, (c) 15 wt% and (d) 20 wt%

We used the dielectric relaxation spectroscopy to investigate the phase separation morphologies of the obtained composite films. Figure 3 shows typical $MgAc_2$ content dependent dielectric spectra of the films cast from different solution mixtures of PLA and $MgAc_2$. The mixing rule proposed by Popielarz *et al.*[21] predicts the effective dielectric permittivity of a composite as follows

$$\lg \varepsilon'_{\text{composite}} = \lg \varepsilon'_{\text{matrix}} + \phi_{\text{filler}} \lg\left(\frac{\varepsilon'_{\text{filler}}}{\varepsilon'_{\text{matrix}}}\right) \tag{1}$$

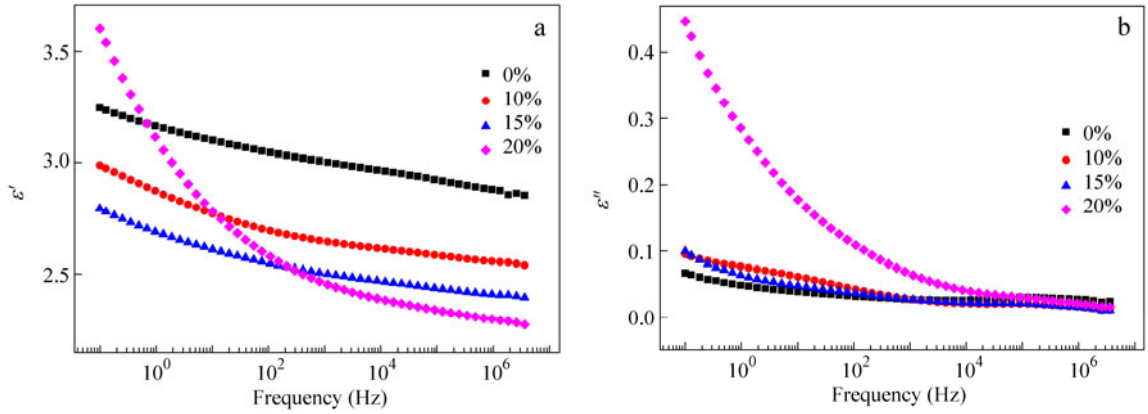

Fig. 3 Frequency dependence of real and imaginary parts (ε' and ε'') of complex permittivity of cast films with different $MgAc_2$ contents

where ϕ_{filler} is the volume fraction of fillers in the composite and $\varepsilon'_{\text{matrix}}$ is the dielectric permittivity of pure polymer matrix without any filler. Therefore, the composite's permittivity should increase with the filler content if $\varepsilon'_{\text{filler}} > \varepsilon'_{\text{matrix}}$. Note that here at high frequencies, $\varepsilon'_{\text{PLA}}$ is *ca.* 3, while $\varepsilon'_{\text{MgAc}_2}$ is *ca.* 8. Unexpectedly, Fig. 3 shows an opposite trend, *i.e.*, the higher the salt content, the lower the high-frequency permittivity, indicating

that $MgAc_2$ induces the formation of domains with a permittivity lower than ε'_{PLA}. Here the only possibility is the formation of voids filled with air that has a lower permittivity, presumably due to the retarded evaporation of water molecules in the $MgAc_2$ phase during the casting process.

In principle, the porosity of each composite can be deduced from its measured permittivity and the volume fractions of PLA and $MgAc_2$ because we know ε'_{PLA}, ε'_{MgAc_2} and ε'_{air}. If we assume both the void and the salt phases are dispersed inside, Eq. (1) can be rewritten as

$$\lg \varepsilon'_{composite} = \lg \varepsilon'_{matrix} + \phi_{filler} \lg\left(\frac{\varepsilon'_{filler}}{\varepsilon'_{matrix}}\right) + \phi_{void} \lg\left(\frac{\varepsilon'_{air}}{\varepsilon'_{matrix}}\right) \quad (2)$$

where ϕ_{void} is the volume fraction of voids inside a composite, *i.e.*, its porosity. Note that the densities of PLA and $MgAc_2$ are 1.250 g/cm^3 and 1.454 g/cm^3, respectively. After knowing the volume ratio between $MgAc_2$ and PLA (ϕ_{filler}), we can deduce the porosity of a given film from the value of ε' at $\omega \to \infty$ using Eq. (2). In the calculation, we used the initial $MgAc_2$/PLA volume ratio as a starting ϕ_{filler} to calculate ϕ_{void} using Eq. (2) and then used this calculated ϕ_{void} to go back to get another ϕ_{filler}. Such iteration was repeated until both ϕ_{filler} and ϕ_{void} became stable. The calculated results for the composite films with the salt content from 1% to 20% are summarized in the second line of Table 1. Composite film made from the aqueous solution of $MgAc_2$ with pH of 7.4 is of as high porosity as 25% for the $MgAc_2$ content of 20 wt%. Such formed macro-porous films are brittle and do not have desired mechanical properties for coating or bracing.

Table 1. Porosities calculated from measured permittivity of composite films

$MgAc_2$ content (wt%)	0%	10%	15%	20%
ϕ_{void} (pH = 7.40)	4%	15%	20%	25%
ϕ_{void} (pH = 4.75)	14%	10%	9%	7%

On the other hand, Fig. 3 shows that in the low-frequency range, both ε' and ε'' remarkably increase when the $MgAc_2$ content reaches 20 wt%, which is from the conduction contribution, indicating the formation of a continuous salt phase. A combination of lower and higher frequency ε' and ε'' data in Fig. 3 makes us to realize that $MgAc_2$ is deposited at the interface of those inter-connected voids.

To lower the porosity of the composite film, we changed the initial pH of the salt solutions before they are mixed with the PLA solutions. We found that the buffer's pH (about 4.5–5.0) of an equal molar mixture of acetic acid and acetate ions provided from $MgAc_2$ is optimal to provide films with least void and best mechanical properties through trial and error, we adjusted the initial pH of the aqueous solution around HAc's pK_a (*ca*. 4.75) before mixing it with the PLA solution, and the porosity calculated from Eq. (2) is listed in the third line of Table 1. As shown in Table 1, the porosity of the composite (15 wt% $MgAc_2$) prepared at pH = 4.75 is 9%, much lower than 20% for the same composite prepared at pH = 7.4. To further explore the influence of pH on the phase morphology of the composite films, we prepared the composite films with the aqueous salt solution of various pH values but at fixed salt content and drying temperatures. The frequency dependences of permittivity of the composite films are shown in Fig. 4.

Figure 4 shows that lowering initial pH of $MgAc_2$ aqueous solution from 7.4 to 3.5 before mixing it with the PLA 1,4-dioxane solution increases the film's permittivity at low frequency, indicating that the domain size of the salt phase increases, while the permittivity in the high frequency range increases with the pH decreasing from 7.4 to 5, and further decrease of pH below 4 leads to a decreasing of the film's permittivity, showing an minimum porosity of the film around pH of 5. It is clear that in the presence of $MgAc_2$, the composite films formed at pH = 4.75 are much less porous.

To search for the mechanism of void control by the pH and salt content, we look through the liquid-liquid phase separation and pore forming process. Although the solvents of water and dioxane is miscible, the salt solution and PLA/dioxane solution is immiscible in the process of drying, namely, with the evaporation of

solvents, there leaves more and more water in the system because of its high vapor pressure, and the liquid-liquid separation occurs. Such phase separation is a kinetic process[22, 23], the coarsening patterns are characterized by the domain length scale as the exponential function of time, $L(t)$ is proportional to t^{Z}. The non-vaporized solvents left in the composite after PLA is solidified will become voids. That's why the final multiphase morphology is hugely affected by the drying rate. In the coarsening process, the exponent Z depends on the physical properties of the liquids, evidence has shown that the interfacial tension is the major driven force[24]. In our opinion, since the pH and the ion concentrations change the surface tension of the salt solution and the interfacial tension between the phases of salt and PLA, which affects the phase separation kinetics, so that the porosity in the final composite film is affected as well.

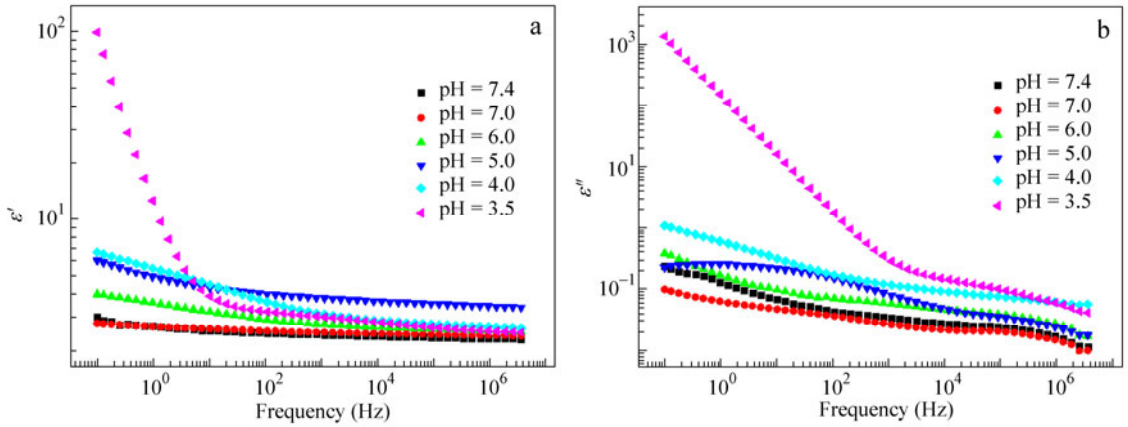

Fig. 4 Frequency dependence of real and imaginary parts (ε' and ε'') of complex permittivity of composite films cast with an identical $MgAc_2$ content (10 wt%) but different initial pH values in $MgAc_2$ aqueous solution at 25 °C

The void assumption is verified by the SEM observations for cryo-fractured cross sections shown in Fig. 5, in which composite film prepared at pH 7.4 provides so high porosity that the voids are connected, those prepared at pH 6.0 and 4.0 show voids with closed pores, and those prepared at pH 4.75 are least porous.

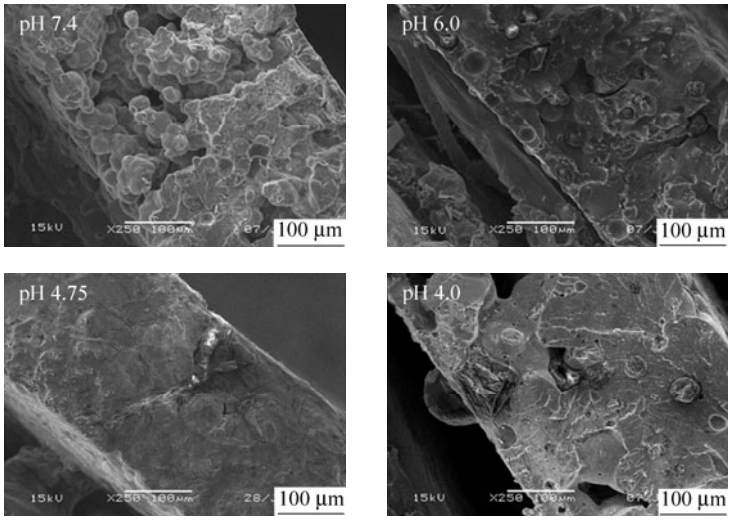

Fig. 5 SEM images of the cross section of the composite films prepared with an identical $MgAc_2$ content (10 wt%) but different initial pH values in $MgAc_2$ aqueous solution

Figure 4 also shows a relaxation peak appeared at *ca*. 10^5 Hz for the films prepared with an initial pH value higher than 6; lowering the initial pH leads to a second peak located at *ca*. 10^2 Hz; and further lowering the initial pH makes a scaling of ε'' with f as ε'' is proportional to f^{υ} and υ is the slope of the line in the double logarithmic plot in the low frequency range, reflecting that conducting over a large scale occurs in the composite film made from low pH. The porosity is higher when the film was prepared at pH either higher than 5 or lower than 4.

Further, we investigated the effect of the volatile temperatures of solvent on the dielectric properties of the PLA/$MgAc_2$ composite films. From the frequency dependent permittivity for the composite films, with fixed solvent component (9:1 *V*/*V*), PLA concentration (0.2 g/mL) and pH of salt solution (4.75), but with varied salt contents and prepared respectively at 30 °C, 50 °C and 70 °C, their high-frequency ε' differs little, but their low frequency ε' sharply increases with the $MgAc_2$ content, indicating the formation of large domains of the salt phase. As discussed above, the high frequency ε' is related to the volume ratios of different components (phases) inside a composite. Here there are polymer, salt and air. While at lower frequencies ε' reflects the film's conductivity. Similar to that shown in Fig. 4, ε'' has a peak at *ca*. 10^5 Hz and ε'' increases as the frequency decreases in the lower frequency range for a given salt content. It also shows that for films with the same salt content, those made at lower evaporating temperature possess higher ε' at a certain frequency.

It also shows that for a given $MgAc_2$ composition, both ε' and ε'' in the low frequency range increase as the drying temperature decreases, *i.e.*, lowering the solvent evaporation rate leads to higher low frequency ε' and ε'', revealing that higher temperatures make the salt phase smaller in the resultant film. Higher temperatures also lead to the films more uniform and with less voids inside, which can be observed from the high frequency permittivity. The salt content dependence of the real part of the permittivity at 1 Hz was plotted by normalizing it with that of the PLA film made at the same condition, the result is shown in Fig. 6. It shows that for a given low frequency, ε' increases with the $MgAc_2$ content in spite of different casting temperatures. In particular, for the composite films cast at the lower temperature (30 °C), ε' substantially increases when the $MgAc_2$ content reaches *ca*. 10 wt%, indicating the formation of $MgAc_2$ regions with large dimension inside PLA. We would analyze how the salt phase morphology changes from the dielectric data. We could of course use the microscopy observation, but that only provides the local information. Since we have fixed the pH of the salt solution, the porosity in the composite changes little with the salt content, the third term at the right of the Eq. (2) can be treated as constant, and an exponential relation between the relative permittivity of composite and matrix and the volume fraction of the filler can be deduced from Eq. (3).

$$\frac{\varepsilon'_{\text{composite}}}{\varepsilon'_{\text{matrix}}} \sim \left(\frac{\varepsilon'_{\text{filler}}}{\varepsilon'_{\text{matrix}}}\right)^{\phi_{\text{filler}}} = 2.67^{\phi_{\text{filler}}} \tag{3}$$

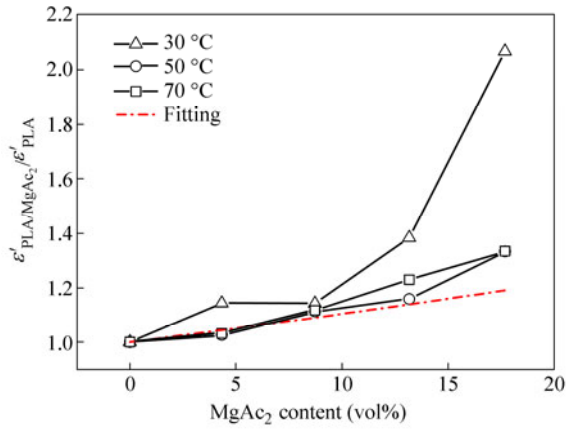

Fig. 6 Salt content dependence of real part of permittivity (ε') of composite films cast at different temperatures but measured at a fixed frequency of 1 Hz (The dash line is the exponential fitting of Eq. (3).)

The $\varepsilon'_{PLA/MgAc_2} / \varepsilon'_{PLA}$ for the composites with low salt content made at 50 °C and 70 °C in Fig. 6 obeys Eq. (3), showing an exponential relation with the volume fraction of the salt in the composite, which can be calculated from the weight ratio, but not for those made at 30 °C. Eq. (1) is established only in the system of 3–0, which means, the minor phase is separated (0 dimension) by the major continuous phase (3 dimension), films with low salt content cast above 50 °C can provide such morphology that the salt phase is isolated from each other, but those with high salt content, especially those made at 30 °C, derivate from the exponential relation. In the cases of high salt content and low drying temperatures there forms the salt phase with dimension higher than 0. It should be noted that the film cast at 70 °C has a slightly lower ε' than that formed at 50 °C for a given PLA/$MgAc_2$ composition, which can be reasonably attributed to the formation of small pores inside the film due to the fast solvent evaporation.

Using the secondary electron imaging (SEI), we can observe the local morphology of the composite films. As shown in Fig. 7, in both the composites made at different temperatures there are porous structures. On the other hand, the back-scattered electron imaging (BSEI) can clearly detect the compositional distribution because the element with a higher atomic mass scatters more electrons and is brighter. Note that the white spherical micro-domains of the salt phase in SEI surface images correspond to those dark areas in BSEI surface images, since the bright area reflects the heavy element of Pt, which is introduced onto the film surface when the Pt plating is performed. It is shown in Fig. 7 that the salt phase is more ball-like (0 dimension) in the composite made at higher temperatures, while for those made at low temperatures, the morphology of the salt phase is of a higher aspect ratio. The quantitative elemental analysis of energy dispersive X-ray spectroscopy (EDS) reveals that the average Mg content in the white areas is *ca*. 0.68 wt%, much less than 1.62 wt% in the original $MgAc_2$ aqueous solution. In contrast, the dark areas with a dimension of 1 μm contains more than 20 wt% Mg. A combination of SEI and BSEI shows that those "balls" in SEI or the dark domains in BSEI are the salt phase because it is difficult to plate $MgAc_2$ with Pt.

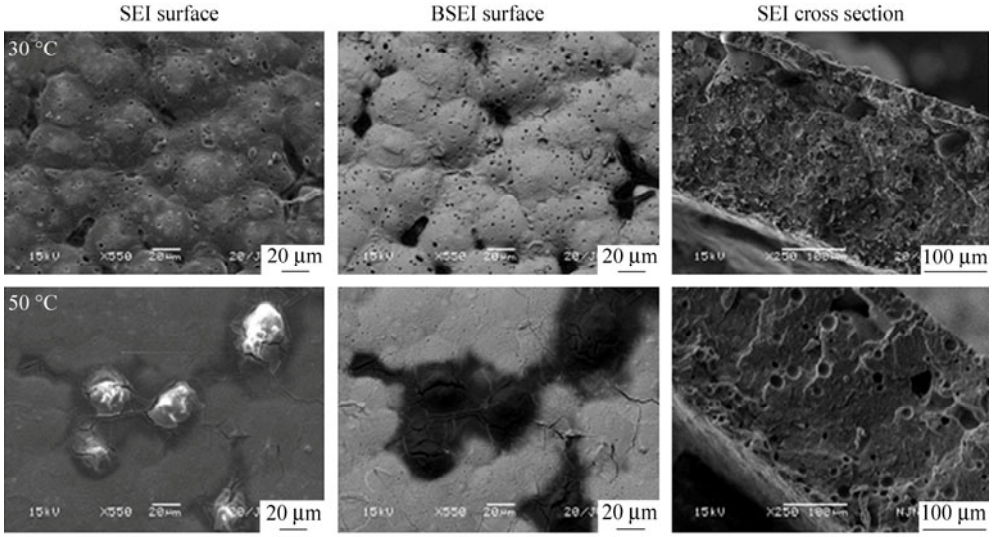

Fig. 7 SEM images of PLA/$MgAc_2$ composite films cast at 30 °C and 50 °C with a fixed $MgAc_2$ content 10 wt% SEI and BSEI stand for secondary and back-scattered electron images, respectively.

After knowing how the salt content, the initial pH in the aqueous salt solution and the evaporating temperature affect the morphology of the composite film, we studied how the $MgAc_2$ embedded in PLA released in water or SBF, and how the salt dissolution is related to the initial film morphology and affects the final film morphology after they dissolve/diffuse out. We used the home-made liquid cell (Fig. 2b) in the dielectric measurement, where one has to make sure that there is no air bubble inside.

Figure 8 shows typical spectra of the real part of permittivity (ε') and the real part of conductivity (σ') during the dissolution of $MgAc_2$, in which both ε' and σ' at a certain frequency increase with the time of immersion in water. For a fixed time, ε' increases while σ' decreases as frequency decreases. The sharp increase of ε' and the moderate decrease of σ' at lower frequency range (< 10^3 Hz) is associated to the electrode polarization. There is a dielectric relaxation observed at 10^4–10^6 Hz, and the plateau value of σ' in the frequency range 10^3–10^5 Hz can be considered as the dc conductivity (σ_{dc}), so that the values of ε' and σ' at *ca*. 10^4 Hz can be used to characterize the dielectric/electric properties of the two-phase system with film and water.

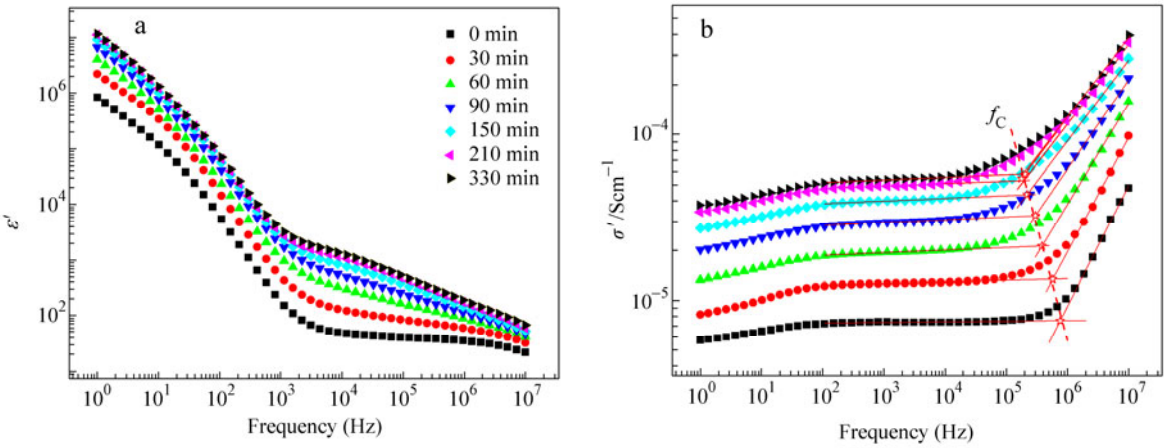

Fig. 8 Frequency dependence of real part of complex permittivity (ε') and conductivity (σ') of a composite film after being immersed in water for different times at room temperature

c_{MgAc_2} = 10 wt%, evaporating temperature was 50 °C, home-made dielectric cell has a dimension of 20 mm (diameter) × 4 mm (thickness).

Figure 8 shows that both ε' and σ' at 10^4 Hz increase with time after the composite film is immerged in water. Initially, the release of $MgAc_2$ is fast, then slows down after *ca*. 10^2 min, and finally stops, presumably because most of the embedded salts are dissolved and diffused out. The intersection of the two lines of the plateau in the frequency range 10^3–10^5 Hz and that at the high frequencies, as shown in Fig. 8, marks the critical frequency f_C at which the dispersion of σ' sets in. Empirically, $2\pi f_C \approx 1/\tau_C$, where τ_C is the characteristic dielectric relaxation time, *i.e.*, the time required for charge carriers to overcome the highest energy barrier to form an infinite cluster of hopping sites that determines the onset of σ_{dc}, according to the random barrier model proposed by Dyre[25] and Kremer[26].

We plotted the changing of τ_C and $\Delta\varepsilon'$ with the releasing time in Fig. 9. It shows that both τ_C and $\Delta\varepsilon'$ quickly increase with time after the composite film is immersed in water and then gradually level off after *ca.* 10^2 min. The inset in Fig. 9 shows that σ_{dc} is scaled to τ_C as $\sigma_{dc} \sim \tau_C^{1.4}$, as predicted by the BNN equation[27, 28], indicating that both the dc- and ac-conductions here are governed by the same charge transport mechanism. We also directly weighted the dried composite film before and after immersing it in the simulated body fluid (SBF) at 37 °C for 100 h. The result shows a total loss of *ca*. 17% mass of the composite film, more than the total mass of $MgAc_2$ embedded inside. Further, we repeated an identical test of a pure PLA film and found that it lost *ca*. 4% of its mass, revealing that PLA also degrades in SBF at 37 °C. The embedded salt actually accelerates the PLA degradation because the salt phase increases the interfacial area.

To confirm the difference is due to the degradation of PLA, we quantitatively analyzed the concentration of Mg^{2+} released into the SBF by using atomic adsorption spectroscopy. First, we established a calibration curve by using a series of standard solutions with known Mg^{2+} concentrations. Second, the SBF solution after 100 h with those released Mg^{2+} was diluted 25 times. The measurements show that it contained Mg^{2+} of 2.4 μg/mL, which means the total amount of Mg^{2+} released in the SBF solution is 3 mmol, *i.e.*, the total released $MgAc_2$ is 9.3 wt% of the film, fairly close to the original $MgAc_2$ content (10 wt%,) in the film.

Finally, we compared the dielectric/electric spectra of those porous films before and after $MgAc_2$ is dissolved/diffused out in water, as shown in Fig. 10. It shows the spectra measured in water, where the dielectric contribution of the Teflon cell used is eliminated by a calibration with its respective cell and real space capacitances of 1.78 pF and 3.68×10^{-1} pF, respectively; and the measured capacitance is treated as a sum of the sample and the cell in parallel. The details of the calibration of such a sample cell can be found in Novocontrol Manuals. Figure 10 shows a clear relaxation mode in both permittivity and conductance spectra in the range 10^3–10^4 Hz, which is attributed to the Maxwell-Wagner-Sillars polarization[13–15], because dielectric effects generated by the applied field on the film and on water do not match or cancel with each other.

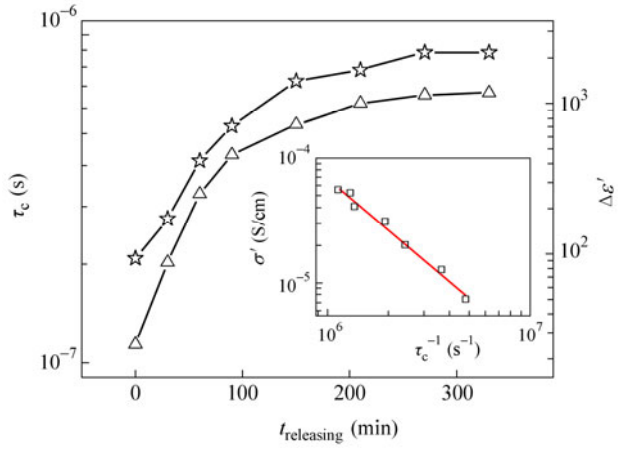

Fig. 9 Time dependence of characteristic relaxation time (τ_C, star) and interfacial polarization induced dielectric increment ($\Delta\varepsilon'$, triangle) of a film (C_{MgAc_2} = 10 wt% and $T_{casting}$ = 50 °C) submerged in water

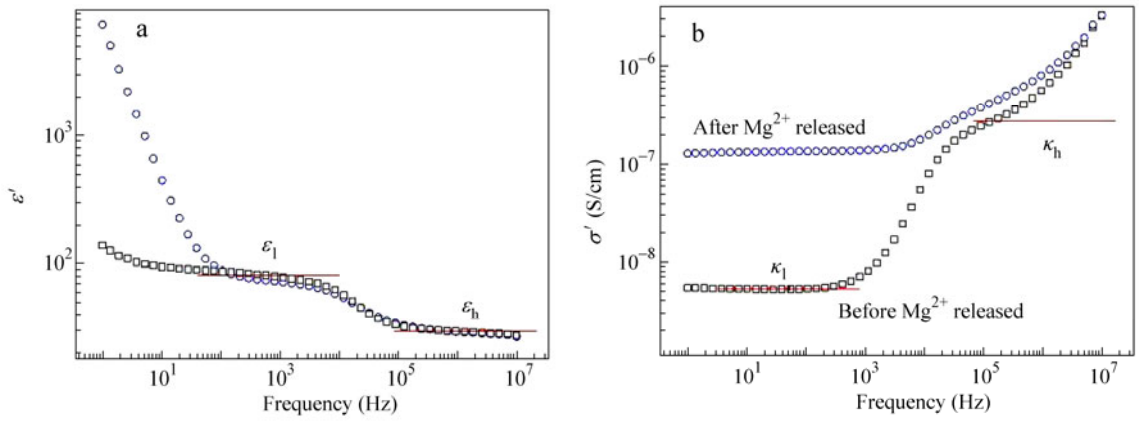

Fig. 10 Frequency dependence of real part of complex permittivity (ε') and conductivity (σ') of films measured in water using liquid cell (C_{MgAc_2} = 10 wt% and $T_{casting}$ = 50 °C)

Figure 11(a) shows a schematic of a film immerged in water, where ε and κ are dielectric and electrical parameters; subscripts *f* and *w* denote the film and water, respectively; and *l* and *d* are the thicknesses of the film and the cell, respectively. In an equivalent circuit, as shown in Fig. 11(b), the water phase can be described by a capacitance (C_w) and admittance (G_w) in parallel circuit. In the low frequency range, there is a universal dielectric response (UDR) in parallel[29], which represents a universal frequency response for the broad low frequency dielectric spectrum, as shown in Fig. 10 at f < 10 Hz. Such a response is omitted in our further calculation because it mainly contributes to the low-frequency conductivity. The film phase can be represented by a capacitance (C_f) and an admittance (G_f) in parallel. In a parallel circuit of elements of C_w, G_w, C_f, and G_f, as shown in Fig. 11(b), their complex capacitances of conductance, C^* and G^* are governed by

$$\frac{1}{C^*} = C + \frac{G}{i\omega} = \frac{1}{C_w^*} + \frac{1}{C_f^*} = \frac{G_w G_f + i\omega(C_w G_f + C_f G_w) - \omega^2 C_w C_f}{i\omega(G_w + G_f)\left(1 + i\omega\dfrac{C_w + C_f}{G_w + G_f}\right)} \tag{4}$$

$$\frac{1}{G^*} = G + i\omega C = \frac{1}{G_w^*} + \frac{1}{G_f^*} = \frac{(G_w + i\omega C_f)\cdot(G_f + i\omega C_w)}{G_w + i\omega C_w + G_f + i\omega C_f} \tag{5}$$

After separating the real and imaginary parts of C^* and G^*, we can get

$$C_h = \frac{C_w \cdot C_f}{C_w + C_f}, C_l = \frac{C_w G_f^2 + C_f G_w^2}{(G_w + G_f)^2}, G_l = \frac{G_w \cdot G_f}{G_w + G_f}, G_h = \frac{G_w C_f^2 + G_f C_w^2}{(C_w + C_f)^2}, \omega_0 = \frac{1}{\tau} = \frac{G_w + G_f}{C_w + C_f} = \frac{G_h - G_l}{C_l - C_h}$$

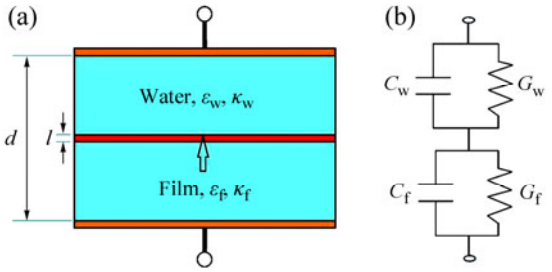

Fig. 11 Schematics of (a) dielectric/electric measurement of a composite film in water and (b) an equivalent circuit of a system consisting of a solid film and a liquid

Using the numerical analysis developed by Hanai[30] for a two-layered system, we are able to calculate these electric parameters (C_w, G_w, C_f, and G_f) from those measured permittivity and conductivity plateau at lower and higher frequencies, *i.e.*, ε_l, κ_l, ε_h and κ_h, as indicated in Fig. 10. Our analysis shows that for the film with embedded $MgAc_2$, $\varepsilon_w = 82$, $\varepsilon_f = 2.8$, $\kappa_w = 1.8 \times 10^{-1}$ μS/m, and $\kappa_f = 2.1$ μS/m; while for the film with voids (*i.e.*, after the removal of Mg^{2+}), $\varepsilon_w = 92$, $\varepsilon_f = 3.5$, $\kappa_w = 15$ μS/m, and $\kappa_f = 7.7$ μS/m. As expected, releasing the salt to water and filling voids of the film with water increase ε and κ of both water and film. From those dielectric/electrical parameters we can use Eq. (2) again to estimate the multi-phase structure of the film while it is in water, assuming the film now is made of PLA, residue salt and void filled with salt water. We also found that the characteristic relaxation time (τ_C) of the polarization at the film/water interface is *ca*. 39 μs and *ca*. 12 μs for the composite films before and after the removal of $MgAc_2$, respectively.

CONCLUSIONS

Using a solution mixture of polylactic acid (PLA) in 1,4-dioxane and $MgAc_2$ in water, we are able to make polymer/inorganic composites (bulk or film) for potential orthopaedic applications, meeting the medical requirements of biodegradability and bioactivity. The releasing of Mg ions *in vivo* can promote the bone-growth, and the generated porous PLA provides scaffold for tissue engineering in orthopaedic therapies. After varying the PLA concentration, the salt content, the solvent composition, the initial pH of the aqueous solution, the standing time after the solution blending, the drying temperature and the solvent evaporation rate, we have found a set of conditions to prepare these PLA/$MgAc_2$ composite films with controllable multi-phase morphologies. The fundamental morphological investigation by using dielectric relaxation spectroscopy, electron microscopes, and atomic adsorption has enriched our understanding of how Mg salts and voids are dispersed in and released from a polymer matrix. Specially, we have used the dielectric relaxation spectroscopy to quantize the porosity in the composite film, evaluate the morphology of the salt phases dispersed in the polymer matrix, and monitor the releasing of the salt in water.

REFERENCES

1 Lasprolla, A.J.R., Martinez, G.A.R., Lunelli, B.H., Jardini, A.L. and Filho, R.M., Biotech. Adv., 2012, 30: 321
2 Chen, Y., Song, Y., Zhang, S., Li, J., Zhao, C. and Zhang, X., Biomed. Mater., 2011, 6: 025005
3 Rezwan, K., Chen, Q.Z., Blaker, J.J. and Boccaccini, A.R., Biomaterials, 2006, 27: 3413
4 Wang, G. and Zreiqat, H., Materials, 2010, 3: 3994
5 Mourin, V., Cattalini, J.P. and Boccaccini, A.R., J. R. Soc. Interface, 2012, 9: 401
6 Zhou, H., Lawrence, J.G. and Bhaduri, S.B., Acta Biomaterialia, 2012, 8: 1999
7 Wang, J., Tang, J., Zhan, P., Li, Y., Wang, J., Lai, Y. and Qin, L., J. Biomed. Mater. Res. B Appl. Biomater, 2012, 100B(6): 1691
8 Gu, X., Xie, X., Li, N., Zheng, Y. and Qin, L., Acta Biomaterialia, 2012, 8: 2360
9 Niki, Y., Matsumoto, H., Suda, Y., Otani, T., Fujikawa, K., Toyama, Y., Hisamori, N. and Nozue, A., Biomaterials, 2003, 24: 1447
10 Vormann, J., Mol. Aspects Med., 2003, 24: 27
11 Balazs, A.C., Emrick, T. and Russell, T.P., Science, 2006, 314: 1107
12 Jancar, J., Douglas, J.F., Starr, F.W., Kumar, S.K., Cassagnau, P., Lesser, A.J., Sternstein, S.S. and Buehler, M.J., Polymer, 2010, 51: 3321
13 Steeman, P.A.M. and van Turnhout, J., in "Broadband Dielectric Spectroscopy", ed. By Kremer, F. and Schonhals, A., Springer, New York, 2003, p. 495
14 Brosseau, C., J. Phys. D: Appl. Phys., 2006, 39: 1277
15 Williams, G. and Thomas, D.K., Novocontrol Application Note Dielectrics, 1998, 3: 1
16 Achour, M.E., Brosseau, C. and Carmona, F., J. Appl. Phys., 2008, 103: 094103
17 Lu, H., Zhang, X. and Zhang, H., J. Appl. Phys., 2006, 100: 054104
18 Zhu, D., Bin, Y. and Matsuo, M., J. Polym. Sci. Part B: Polym. Phys., 2007, 45: 1037
19 Zhu, D., Zhang, J., Bin, Y., Xu, C., Shen, J. and Matsuo, M., J. Phys. Chem. A, 2012, 116: 2024
20 Tanaka, T. and Lloyd, D.R., J. Membr. Sci., 2004, 238: 65
21 Popielarz, R., Chiang, C.K., Nozaki, R. and Obrzut, J., Macromolecules, 2001, 34: 5910
22 Haas, C.K. and Torkelson, J.M., Phys. Rev. E, 1997, 55: 3191
23 Tanaka, H., Phys. Rev. Lett., 1994, 72: 1702
24 McMaster, L.P., in "Copolymers, Polyblends, and Composites, Vol. 142", ed. by Platzer, N.A.J., ACS, New York, 1975, p. 43
25 Dyre, J.C., J. Appl. Phys., 1988, 64: 2456
26 Kremer, F., Dielectric Newsletter, 2002, Issue April: 4
27 Wubbenhorst, M. and van Turnhout, J., Dielectric Newsletter, 2000, Issue November: 1
28 Namikawa, H., J. Non-Cryst. Sol., 1975, 18: 173
29 Jonscher, A.K., Nature, 1977, 267: 673
30 Hanai, T., "The heterogeneous structure and the permittivity" (in Japanese), Yoshioka, Tokyo, 1999, p. 61